Applied Catalysis B: Environmental 134–135 (2013) 136–144

Contents lists available at SciVerse ScienceDirect

Applied Catalysis B: Environmental

journal homepage: www.elsevier.com/locate/apcatb

Low-temperature ultrasound-promoted synthesis of Cr–TiO_2-supported photocatalysts for valorization of glucose and phenol degradation from liquid phase

Juan C. Colmenares[a,*], Agnieszka Magdziarz[a], Krzysztof Kurzydlowski[b], Justyna Grzonka[b], Olga Chernyayeva[a], Dmytro Lisovytskiy[a]

[a] Institute of Physical Chemistry PAS, Kasprzaka 44/52, 01-224 Warsaw, Poland
[b] Faculty of Materials Science and Engineering, Warsaw University of Technology, Woloska 141, 02-507 Warsaw, Poland

ARTICLE INFO

Article history:
Received 9 October 2012
Received in revised form 10 January 2013
Accepted 14 January 2013
Available online 23 January 2013

Keywords:
Selective glucose photo-oxidation
Phenol mineralization
Sonication
Ultrasound-assisted impregnation
Cr–TiO_2
Solar chemicals

ABSTRACT

Novel chromium doped titania zeolite or silica supported photocatalysts were prepared via ultrasonically modified wet impregnation method. In this method, rotary evaporator was coupled with ultrasonic bath. The resulting nanomaterials were characterized by several techniques such as XRD, DR UV–vis, N_2 physisorption, XPS, ICP-MS, XRF, HRTEM–EDS and they were subsequently tested for their photocatalytic activities in liquid phase processes: selective oxidation of glucose and total mineralization of phenol. Two carboxylic acids (glucaric acid and gluconic acid) were detected as the liquid phase products in the glucose photo-oxidation and better selectivity was achieved for the photocatalyst supported on zeolite. In phenol photodegradation, although conversion rate was not meaningful (ca. 30% after 4 h illumination time), negligible amounts of harmful phenol-derived compounds were detected in water compared with photodegradation using the commercial P-25 photocatalyst. This ultrasonically improved photocatalysts synthesis method was found to have a significant effect on textural properties, spherical shape, good dispersion and visible-light responsiveness of nanophotocatalysts.

1. Introduction

Among many problems affecting our modern society environmental pollution is one of the most disturbing. For many years researchers have been looking for an attractive method of decontaminating polluted water and air. Hence, semiconductor photocatalysis, due to its efficiency and promising economy, seems to come up to some expectations in this field [1]. When we think about photocatalysis, titanium dioxide comes directly to our minds as it is still the most relevant photocatalytic material. Besides unquestionable advantages that it presents, like low level of toxicity, low cost, photo-stability, redox efficiency and availability, there are still some important drawbacks that must be overcome to make it completely efficient for technological purposes. The major drawback is the fact that TiO_2 does not absorb wavelengths above 370 nm due to its wide band gap at about 3.2 eV, what makes it photocatalytically ineffective under visible light [2]. In consequence, only ca. 5% of solar light can be absorbed during this photocatalytic process. Thus for, there is strong research effort aiming to shift the absorption of TiO_2 from the ultraviolet to visible light range. One of the typical approaches to extend the activity of TiO_2 is its modification with metal or non-metal ions. These ions are employed to tune the electronic structure of TiO_2 by introducing a donor and/or acceptor level in the wide forbidden band of TiO_2. That allows photons with some lower energy to excite photocatalyst and exhibit a visible light photocatalytic activity [3]. Among these transition metals, Cr^{3+} has received a significant attention due to its properties and was widely studied [4–7]. Moreover, another limitation is the practical use of "bare" nanostructured TiO_2 in photocatalytic reactors, due to the fact that TiO_2 particles aggregate rapidly in suspension, resulting in smaller effective surface area and lower catalytic efficiency. Small size of TiO_2 particles also complicates the filtration of suspensions, making slurry photocatalytic reactors impractical [8]. Therefore, numerous methods were suggested (e.g. sol–gel, hydrothermal, chemical vapor deposition) for anchoring fine TiO_2 particles on supports with the aim of easy handling as well as to improve reagents adsorption and photocatalytic efficiency [9,10]. From the group of supports, zeolites and silica distinguish themselves due to their photocatalytically attractive features such as good pollutant adsorption, diffusion properties and absence of light absorption [11]. Additionally, zeolites have been reported to delocalize band gap excited electrons of TiO_2 and thereby minimize electron–hole recombination as if to favor photoinduced electron-transfer reactions [12].

* Corresponding author. Tel.: +48 22 343 3215.
E-mail address: jcarloscolmenares@ichf.edu.pl (J.C. Colmenares).

0926-3373/$ – see front matter © 2013 Elsevier B.V. All rights reserved.
http://dx.doi.org/10.1016/j.apcatb.2013.01.020

Wood residues (including sawmill and paper mill discards) and municipal paper waste provide a great amount of lignocellulosic biomass that contaminate water. Conversion of this abundant material into renewable chemicals and fuels has received significant attention as a mean to the sustainable society [13]. Various methods have already been developed for biomass reforming processes [14–16], however among them, photocatalysis deserves particular attention, because the reaction conditions are mild and can be carried out at ambient temperature under solar irradiation [17].

In the present work, the synthesis of nanometer-sized spherical titania particles with narrow size distribution through the ultrasound-assisted impregnation of metal (Ti, Cr) organic precursors into well defined inorganic supports is reported. It is already known that ultrasonic irradiation provides rather unusual reaction conditions (extremely high temperatures and pressures form quickly in liquids due to cavitation phenomena) that cannot be realized by other methods. More uniform dispersion of nanoparticles, higher surface area, better thermal stability and phase purity are some of the advantages of sonication method [18]. Therefore, ultrasound treatment has already been coupled with different synthesis techniques [19–21], among others with wet impregnation method [22,23]. However, in referred reports ultrasonic irradiation has been applied only before solvent evaporation. Herein, in the proposed environmental friendly methodology, ultrasound treatment is also implemented during the solvent evaporation step.

The selected chemical transformations, as proof of concept for photocatalytic activity, include the liquid phase selective photocatalytic oxidation of glucose to glucaric and gluconic acids under mild conditions and the total photocatalytic mineralization of phenol in water also under no-drastic conditions.

2. Experimental

All chemicals were used as received without further purification.

2.1. Synthesis of materials

Two different photocatalysts modified with chromium were prepared: Cr–TiO_2 supported on fumed silica AEROSIL 200 (denominated as Cr–TiO_2/SiO_2UI) and Cr–TiO_2 supported on zeolite CBV 780 (denominated as Cr–TiO_2/ZeUI). Zeolite and silica before the synthesis procedure were thermally treated at 450 °C during 8 h in static air. A simple, wet impregnation method assisted by ultrasonic irradiation was applied to synthesize these materials. The procedure began with the addition of 5.35 mM of titanium (IV) isopropoxide (TTIP) into an isopropanol (70 mL) solution at room temperature. Next, ca. 2 g of PEG (M.W. 400) and 2.5 g of zeolite Y was added into isopropanol-TTIP mixture. After that, Cr precursor solution (0.5 mM of $C_{15}H_{21}CrO_6$ in 10 mL of isopropanol) was added and such mixture was treated with ultrasound (operating frequency 35 kHz, 560 W, Sonorex Digitec-RC, Bandelin) for 60 min. Then, the solvent was slowly evaporated (at the temperature ca. 50 °C) by a rotary evaporator coupled with ultrasonic treatment (the water bath was replaced by ultrasonic bath, see graphical abstract). The solid material was further dried for 4 h at 110 °C and finally calcined at 500 °C in 30 mL/min air flow for 4 h to remove organic precursors. Chromium content was adjusted to a nominal mass percentage of 1%, while nominal quantity of titanium dioxide was fixed on 15%.

The synthesis of silica supported samples was conducted in a similar way, while the amount of silica AEROSIL 200 taken to this synthesis was 3 g. Proportions of chemicals were preserved.

2.2. Materials characterization

Powder XRD measurements were performed using standard Bragg–Brentano configuration. This type of arrangement was provided using Siemens D5000 diffractometer (equipped with a horizontal goniometer) with θ–2θ geometry and Ni filtered Cu Kα radiation, powered at 40 kV and 40 mA. Data were collected in the range of 2θ = 10–90° (some data up to 120°) with step interval of 0.02° and counting time up to 5 s per step.

Elementary compositions of samples were determined using the energy dispersive X-ray fluorescence (EDXRF) spectrometer (MiniPal 4, PANalytical&Co.) with Rh tube and silicon drift detector. The spectra were collected in air atmosphere, without using a filter, at a tube voltage of 30 kV. The time of acquisition was set to 30 s and the tube current up to 50 μA.

The ICP-MS measurements were performed using Elan 6100 DRC SciexPerkinElmer spectrometer. Before the analysis samples were mineralized in the mixture of H_2SO_4, HF and H_2O_2 (2:2:2 mL v/v). Determination of the elements was carried out from the corresponding calibration curves.

Nitrogen adsorption–desorption was measured with Micromeritics instrument model ASAP 2020 at −196 °C. Prior to the measurements the samples were outgassed twice under vacuum, firstly at 350 °C for 8 h and secondly, in the sample port, at 300 °C for 4 h. The surface area was calculated using the Brunauer–Emmett–Teller (BET) method and the pore size by the Barret–Joyner–Halenda (BJH) and Horvath–Kawazoe (H–K) method for silica supported samples and zeolite supported samples, respectively.

Band gap energies of samples were determined using UV–vis diffuse reflectance (DRS) with a UV-2501 PC Schimadzu spectrophotometer equipped with an integrating sphere in the range of 200–900 nm using $BaSO_4$ as a reference. The Kubelka–Munk function, $f(R)$, was considered proportional to the absorption of radiation and band gap energy, E_g, of the semiconductor TiO_2 was evaluated from the DRS spectra by plotting $[f(R)h\nu)]^{1/2}$ against $h\nu$. The function $f(R)$ was calculating using the equation [24]:

$$f(R) = \frac{(1-R)^2}{2R} \tag{1}$$

The structure characterization of powders was carried out with high resolution scanning transmission electron microscope (STEM, Hitachi HD-2700, 200 kV, C_s corrected) with energy dispersive X-ray spectrometer. The samples for STEM observations were prepared through mixing powder with ethanol using ultrasonic washing and then dropping on copper grids covered with carbon film. After alcohol evaporation the samples were ready for micrographs recording.

The XPS measurements were performed using a VG Scientific photoelectron spectrometer ESCALAB-210 using Al Kα radiation (1486.6 eV) from an X-ray source operating at 15 kV and 20 mA. Survey spectra were recorded for all the samples in the energy range from 0 to 1350 eV with 0.4 eV step. High resolution spectra were recorded with 0.1 eV step, 100 ms dwell time and 25 eV pass energy. Ninety degrees take-off angle was used in all measurements. The curve fitting was performed using the AVANTAGE software provided by Thermo Electron, which describes each component of the complex envelope as a Gaussian–Lorentzian sum function; a constant 0.3(±0.05) G/L ratio was used. The background was fitted using nonlinear Shirley model. Scofield sensitivity factors and measured transmission function were used for quantification. Aromatic carbon C 1s peak at 284.5 eV was used as reference of binding energy.

2.3. Photocatalytic experiments

All photocatalytic tests were performed in a Pyrex cylindrical double-walled immersion well reactor with a total volume of 450 mL.

2.3.1. Liquid-phase selective photo-oxidation of glucose

The bath reactor was stirred magnetically to obtain a homogenous suspension of the catalyst. The suspension was first maintained in the dark for 20 min to reach complete adsorption equilibrium of glucose on the photocatalyst surface. A medium pressure 125 W mercury lamp (λ_{max} = 365 nm), as a light source, supplied by Photochemical Reactors Ltd. (Model RQ 3010) was placed inside the borosilicate glass immersion well (300 nm, wavelength at which a 1 mm layer of the glass absorbs at least 90% the light). The reaction temperature was 30 °C. Glucose solution (2.8 mmol/L) was prepared in a mixture of Milli-Q water and acetonitrile (10:90 v/v), unless otherwise specified. Experiments were carried out from 150 mL of mother solution and a concentration of 1 g/L of the catalyst was used. All reactions were carried out under ambient air (no oxygen bubbling conditions). Approx. 2 mL of samples were periodically taken from the photoreactor at specified times and filtered through 0.2 μm, 25 mm nylon filters in order to remove photocatalyst particles before high-performance liquid chromatograph (HPLC) analysis. Glucose conversion and organic products were measured, after calibration, by HPLC (Waters HPLC Model 590 pump), equipped with a refractive index detector (Waters 2414 Refractive Index Detector). Separation was performed on a XBridge™ Amide 3.5 μm 4.6 × 150 mm column provided by Waters. The mobile phase was Milli-Q water/acetonitrile (15:85 v/v) at a flow rate of 0.8 mL/min. The injection volume was 10 μL. All reaction products were identified by gas chromatography–mass spectrometry (GC–MS, Hewlett Packard GC 6890 Series and MS 5973, Hewlett Packard–5 column) after silylation, using N,O-bis(trimethylsilyl)trifluoroacetamide with 1% trimethylchlorosilane as derivatizating agent, performed at 60 °C for 1 h in a CSB/COD-Reaktor ET 108. All products identified by GC–MS were confirmed by liquid chromatography–mass spectrometry (LC–MS, LC Prominence Shimadzu coupled with MS 4000 Q-TRAP Applied Biosystems).

2.3.2. Aqueous phase photodegradation of phenol

All photocatalytic tests with phenol were performed in the setup described above (*for photoselective oxidation of glucose*). The lamp was placed in a borosilicate glass immersion well in order to avoid auto-degradation of phenol (it was observed phenol disappearance under UV irradiation up to 300 nm, Fig. 1, inset). Phenol solution (50 ppm) was prepared in Milli-Q water. Reactions were carried out under ambient air. Phenol degradation was measured, after external standard calibration, by HPLC (Waters HPLC Model 590 pump), equipped with a PDA detector. Separation was performed on a XBridge™ C18 5 μm 4.6 × 150 mm column provided by Waters. The mobile phase was Milli-Q water/methanol (65:55 v/v) mixture with 0.1% of CF_3COOH at a flow rate of 1 mL/min. The injection volume was 10 μL. All intermediates were identified by liquid chromatography–mass spectrometry (LC–MS, LC Prominence Shimadzu coupled with MS 4000 Q-TRAP Applied Biosystems).

Different control experiments, single UV experiments (photolysis) and single adsorption dark experiments, were performed to confirm that these photocatalytic reactions depended on the presence of both, light and photocatalyst. In Fig. 1, it is shown the whole spectrum of the medium pressure mercury lamp used in this investigation (courtesy of Photochemical Reactors Ltd., UK). It was observed that photolysis reactions leaded to a very low conversion in both test reactions in the case of borosilicate glass immersion well (Fig. 1, inset). In phenol degradation, the conversion was approx. 11% after 120 min of illumination and in the case of glucose it was approx. 6% after 120 min. In quartz immersion well

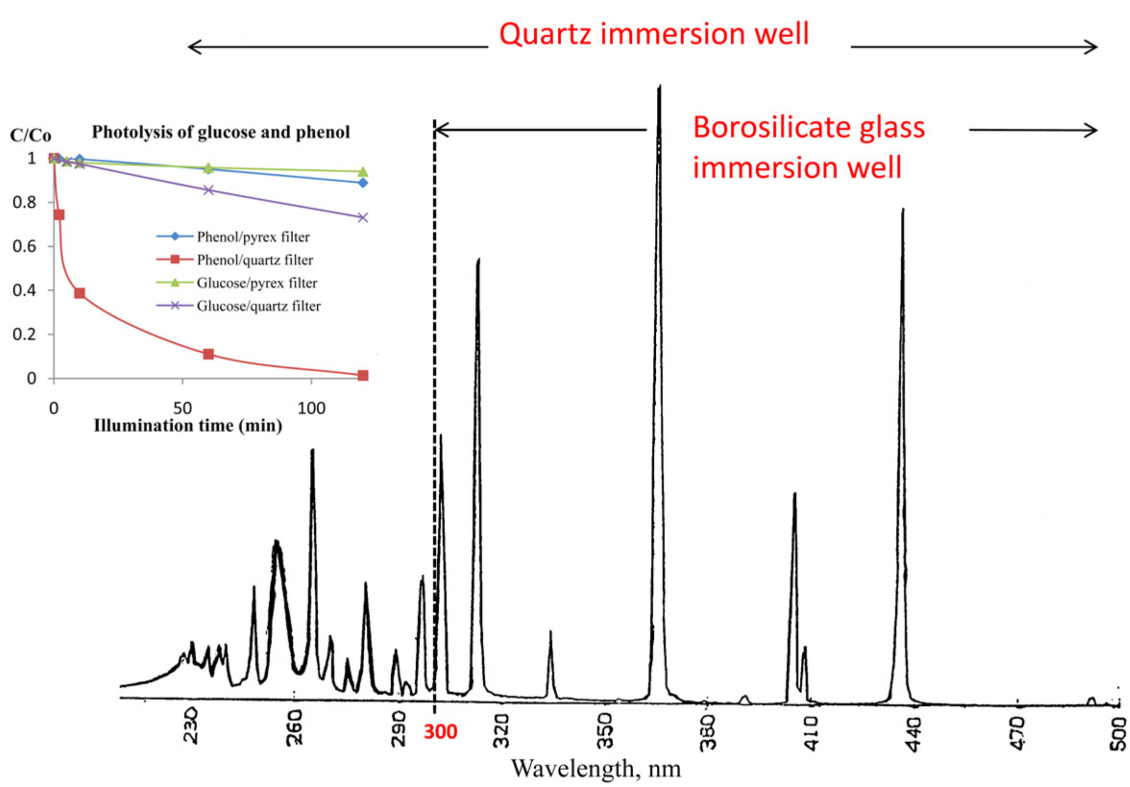

Fig. 1. Spectral output of the medium pressure mercury lamp used in this investigation, supplied by Photochemical Reactors Ltd., UK (inset: effect of light filter used in phenol and glucose photolysis).

Table 1
Structural and textural properties of the synthesized photocatalysts: $Cr–TiO_2/ZeUI$ and $Cr–TiO_2/SiO_2UI$ compared with $TiO_2/ZeUI$ and TiO_2/SiO_2UI.

Material	XRD		N_2-isotherms		
	Crystallite size (nm)	Crystal phase (%)	S_{BET}[a](m^2/g)	V_p[a](mL/g)	d_p[a](nm)
$Cr–TiO_2/ZeUI$	16.5	Anatase (100)	672	0.44	0.7
$Cr–TiO_2/SiO_2UI$	6.6	Anatase (100)	204	0.51	16
$TiO_2/ZeUI$	13.1	Anatase (100)	700	0.49	0.8
TiO_2/SiO_2UI	5.7	Anatase (100)	206	0.75	14.6
Zeolite Y (Ze)	–	–	784	0.52	0.8
SiO_2	–	–	197	0.39	14

[a] Specific surface area (S_{BET}), cumulative pore volume (V_p), median pore width (d_p) was calculated by Barret–Joyner–Halenda (BJH) formula in the case of mesoporous SiO_2 supported samples and Horvath–Kawazoe (H–K) formula for microporous zeolite supported samples.

approximately 30% of glucose and 100% degradation of phenol was achieved after the same illumination time. Dark experiments (in the absence of lamp) provided no conversion of starting material after 2 h of catalyst and reagent contact time.

3. Results and discussion

3.1. Photocatalysts characterization

The XRD patterns (results not shown here) for both photocatalysts showed only the peaks of anatase phase of TiO_2. No diffraction lines for chromium species were detected suggesting that chromium loading and particle size are below the detection limit of this technique [25]. Moreover, the insertion of Cr^{3+} cations in TiO_2 lattice, due to the similar ionic radius of Ti^{4+} (0.68 Å) and Cr^{3+} (0.69 Å), or the formation on titania surface of highly dispersed chromium oxide conglomerates are probable [26]. The crystallite size was estimated from the full width half maximum (FWHM) of the (1 0 1) plane of anatase using the Scherrer formula and it was found to be 16.5 nm for $Cr–TiO_2/ZeUI$ and 6.6 nm for $Cr–TiO_2/SiO_2UI$ (Table 1). From the XRD patterns it was also seen that the TiO_2 diffraction peak in the silica sample was broader than the corresponding one in zeolite sample, which indicates its smaller size. It may suggest, that silica matrix restrains the growth of the TiO_2 crystallites.

The anatase phase in $Cr–TiO_2/ZeUI$ sample has also been confirmed by HRTEM measurements. Separation between lattice fringes has been calculated (Fig. 2(3)) and it was estimated to be 3.66 Å that correspond to the lattice spacing of (1 0 1) of anatase TiO_2. In the Fig. 2(1) zeolite substrate (support) covered with titania oxide particles is seen. Observations performed at higher magnifications (Fig. 2 (2)) helped to reveal the shape and size of titania particles. It has been found that they are mostly spherically shaped and their average size is about 10 nm. This spherical shape could be recognized as the result of the application of ultrasonic treatment during the synthesis procedure. The TEM–EDS spectrum and mapping of all elements are shown in the Fig. 2(4)b–f. A good dispersion of chromium elements is clearly seen (Fig. 2(4)e). However, titania particles revealed some tendency to form agglomerates. EDS

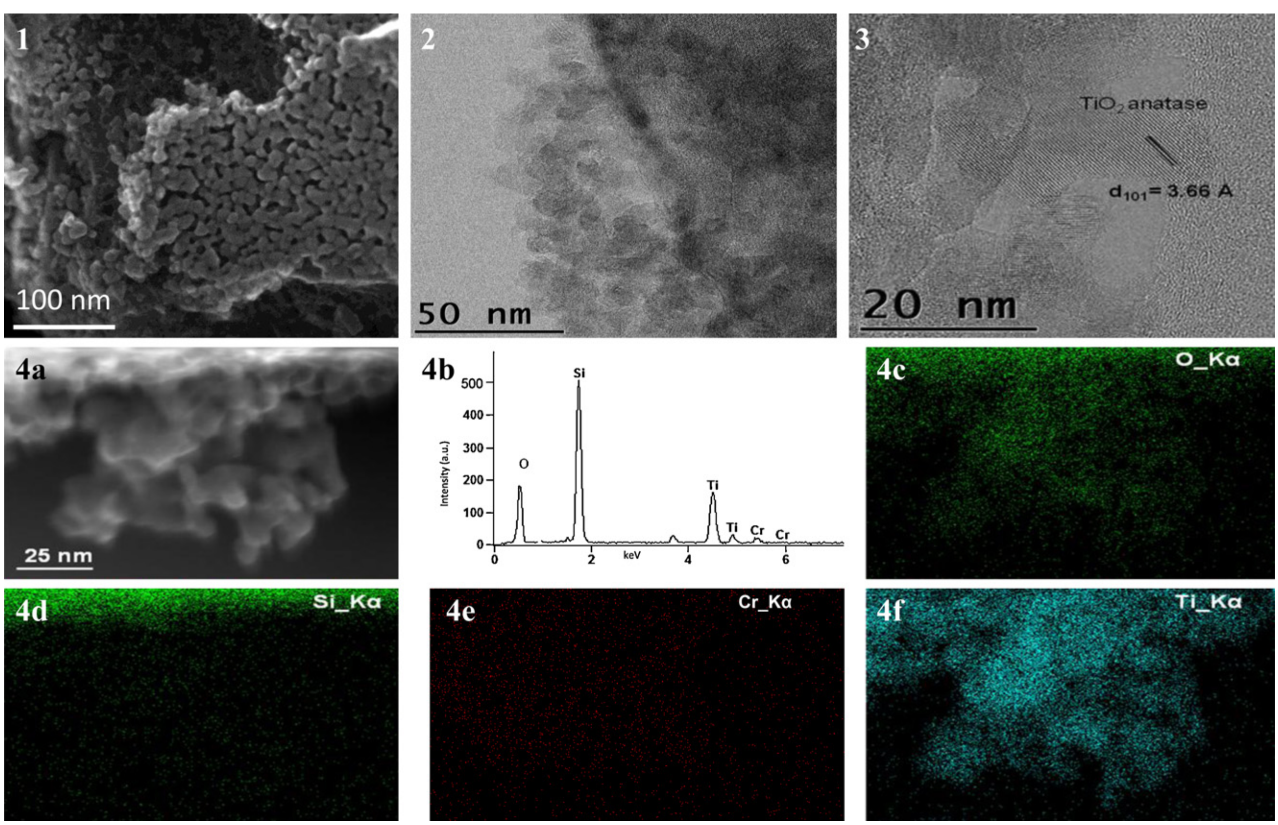

Fig. 2. TEM images of $Cr–TiO_2/ZeUI$: (1) SE image of zeolite substrate covered with oxide particles (2) BF STEM image of oxide particles attached to edge of zeolite substrate, (3) HR STEM image, (4): (a) HAADF STEM image, (b) EDS spectrum, EDS distribution maps of (c) O, (d) Si, (e) Cr, and (f) Ti.

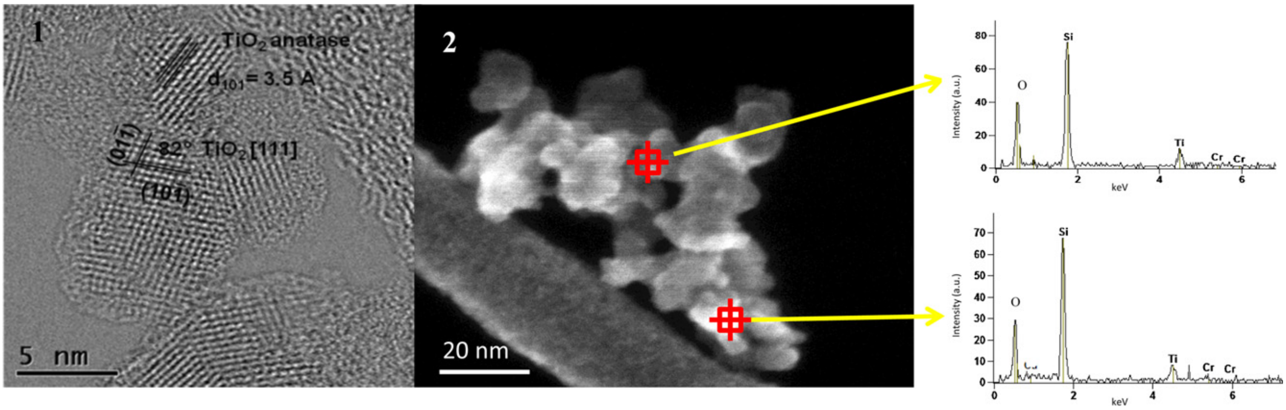

Fig. 3. TEM images for Cr–TiO_2/SiO_2UI: (1) HR STEM images of oxide particles attached to edge of silica substrate, (2) EDS point analysis with HAADF STEM image showing the place of analysis.

Table 2
Band gap values calculated for Cr–TiO_2/ZeUI, Cr–TiO_2/SiO_2UI compared with TiO_2/ZeUI and TiO_2/SiO_2UI.

Photocatalyst	TiO_2		Cr oxidized species	
	E_{gap} (eV)	Absorption threshold (nm)	E_{gap} (eV)	Absorption threshold (nm)
TiO_2/ZeUI	3.27	379	–	–
TiO_2/SiO_2UI	3.31	375	–	–
Cr–TiO_2/ZeUI	3.04	408	2.15	577
Cr–TiO_2/SiO_2UI	3.05	407	2.16	574

analysis confirmed that the proposed wet impregnation synthesis method permits the incorporation of all desired elements on surface supports and the application of ultrasonic irradiation ensures generally their good dispersion.

On TEM images for Cr–TiO_2/SiO_2UI an amorphous phase of SiO_2 is visible, and it could be the reason of poor visibility of TiO_2 crystallite phase. However, magnification of the area helped to define present phase. In the Fig. 3(1) two dimensional lattice fringes with separations of 3.52 Å and 3.52 Å, which correspond to the lattice spacing of $(0\ 1\ \bar{1})$ and $(1\ 0\ \bar{1})$, respectively, of TiO_2 are visible. The measured values indicate presence of TiO_2 anatase phase with [1 1 1] zone axis. The size of nanoparticles has been estimated to be below 10 nm, in well accordance with XRD calculation (6.6 nm). Also spherical shape of particles can be observed. The EDS (Fig. 3(2)) point analysis indicated presence of silicon, oxygen, titanium and chromium elements which is in agreement with the initial composition of powder.

DR UV–vis spectra (Fig. 4) of synthesized Cr-doped samples shows the extension of the absorption band to the visible region in comparison with non doped samples. This significant improvement of the absorption of TiO_2 in the visible light region is obviously correlated with the presence of Cr species and has already been widely discussed [14,26]. In the literature the absorption around 450 nm is generally ascribed to the charge transfer band $Cr^{3+} \rightarrow Ti^{4+}$ or ${}^4A_{2g} \rightarrow {}^4T_{1g}$ of Cr^{3+} in an octahedral environment, while the broad absorption band from 620 to 800 nm can be a result of ${}^4A_{2g} \rightarrow {}^4T_{2g}$ d–d transitions of Cr^{3+} [3,27]. The band gap energies (E_g) of the samples calculated on the base of Kubelka–Munk theory are summarized in the Table 2. The calculated values show that doping Cr slightly reduce the band gap of TiO_2 to the value 3.04 and 3.05 eV for Cr–TiO_2/ZeUI and Cr–TiO_2/SiO_2UI, respectively (comparing with generally accepted 3.2 eV for anatase TiO_2). This red-shift has been attributed by Choi et al. to the localized states near the conduction or valence band of the modified semiconductor [28]. Moreover, it has also been assigned to the formation of color centers, which were associated with the oxygen vacancies in pure TiO_2 or to the radicals in the TiO_2 lattice associated with the doping ions [29]. The Cr–TiO_2/support powders with a doping content of 1.0 wt.% are yellow colored with a slight greeny shade, what indicates a variation in Cr^{3+}/Cr^{6+} ratio. This observation correlates well with XPS commented later. Hence, during the photocatalysts synthesis the Cr (III) from the precursor salt was partially oxidized to Cr (VI).

Textural properties of synthesized materials are summarized in Table 1. Loading of TiO_2 particles on zeolite and doping with Cr ions resulted in the reduction of the surface area and pore volume of the material. It means that TiO_2 nanoparticles probably do not enter in the pores of zeolite and they are more likely embedded in the external surface area of the support (results also confirmed by HRTEM, Fig. 2(1)). Decrease of the specific surface area can be attributed to the growth of TiO_2 particles [25]. In the case of loading of TiO_2 particles on silica and doping with Cr ions, the surface area and pore volume of the material slightly increased. It may suggest an aggregation of TiO_2 particles on the silica surface and the development of voids in this aggregation that might create an additional pore volume [8].

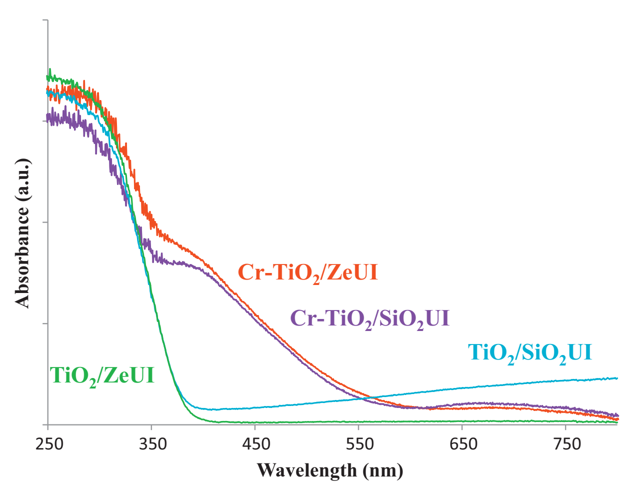

Fig. 4. DR UV–vis absorption spectra of Cr–TiO_2/ZeUI, and Cr–TiO_2/SiO_2UI compared with TiO_2/ZeUI and TiO_2/SiO_2UI.

Table 3
Surface composition and electronic states for Cr–TiO_2/ZeUI and Cr–TiO_2/SiO_2UI by XPS analyses.

Photocatalyst	B.E. (eV)					
	Ti $2p_{3/2}$	Suggested specie (%)	Cr $2p_{3/2}$	Suggested specie (%)	O 1s[a]	Suggested specie[a] (%)
Cr–TiO_2/ZeUI	457.62	Ti^{3+}(23)	576.83	Cr^{3+} (59)	530.03	Ti–O (41)
	458.92	Ti^{4+}(77)	579.34	Cr^{6+} (41)	531.79	Cr–O (59)
Cr–TiO_2/SiO_2UI	457.62	Ti^{3+} (27)	574.05	$Cr^{1.7+}$ (18)	530.96	Ti–O–Cr (100)
	459.18	Ti^{4+} (73)	578.18	Cr^{6+} (82)		

[a] Metal-O bonds concerned.

XPS analysis was employed to determine the surface composition of the photocatalyst elements and their electronic states. From the survey spectra (Fig. 5) the presence of Ti, O, Cr, Si elements is confirmed in both samples. All complete spectra (survey) were calibrated at the C 1s peak (284.5 eV). The Cr $2p_{3/2}$ and Ti $2p_{3/2}$ binding energy (BE) corresponding to oxidation states are presented in Table 3. The binding energy of 458.92 eV for Cr–TiO_2/ZeUI and 459.18 eV for Cr–TiO_2/SiO_2UI correspond to the value of Ti^{4+} in the TiO_2 lattice. Besides, the value of 457.62 for both samples indicates also the presence of Ti^{3+} ions in the TiO_2 lattice (Ti^{4+}:Ti^{3+} = 77:23 for Cr–TiO_2/ZeUI and Ti^{4+}:Ti^{3+} = 73:27 for Cr–TiO_2/SiO_2UI). From the deconvoluted XPS spectrum for Cr–TiO_2/ZeUI we have found that mixed oxidation states of chromium (Cr^{3+}:Cr^{6+}) are present in this sample. Similar results were presented by Wang et al. [25] and Lopez et al. [26] and they claimed that the initial precursor Cr (III) was partially oxidated to Cr (VI) during the synthesis procedure. The Cr^{3+}:Cr^{6+} surface atomic ratio in Cr–TiO_2/ZeUI is equal to Cr^{3+}:Cr^{6+} = 59:41. The signal for O 1s shows two peaks located at 530.03 eV and 531.79 eV which corresponds to the Ti–O and Cr–O bonds, respectively. It suggests that chromium is not incorporated in the titania lattice, but rather forms chromium oxides on the surface. Cr spectrum in the case of Cr–TiO_2/SiO_2UI photocatalyst indicates that $Cr^{1.7+}$:Cr^{6+} mixture is present in the sample in the surface atomic ratio of 18:82. Herein, probably chromium carbide Cr_7C_3 was formed due to the reaction between chromium and carbon (detected by XPS and presumably coming from the organic precursors not completely removed after calcinations step) during the calcination treatment. Firstly, the binding energy for Cr species has been estimated to the value 574.05 eV, which is very close to 574.2 eV, the binding energy of Cr_7C_3. Secondly, the content of carbon, XPS detected, in Cr–TiO_2/SiO_2UI is lower than in Cr–TiO_2/ZeUI (1.61% and 3.89%, respectively), what could confirm the consumption of carbon in carbide compound formation. O 1s peak at 530.96 eV ascribed to Ti–O and Cr–O bonds indicates the presence of Ti–O–Cr junctions.

The bulk elemental analysis was done using XRF and ICP-MS techniques. The Cr/Ti atomic ratios evaluated from both techniques are indicated in Table 4 and they are congruent with the nominal content implying the successful incorporation of Cr into the TiO_2-support samples by the proposed ultrasound methodology. Additionally, Cr/Ti atomic ratio has been calculated in the surface of the materials indicating that the surface is significantly enriched with chromium, especially in the case of Cr–TiO_2/SiO_2UI sample (Cr/Ti = 0.43).

3.2. Photocatalysis

3.2.1. Liquid-phase selective photo-oxidation of glucose

To the best of our knowledge, there are no systematic studies on selective photocatalytic oxidation of glucose, most of the studies regards the photocatalytic reforming of glucose in liquid phase for hydrogen production [30–32].

Two carboxylic acids were the main reaction products in the liquid phase: glucaric acid (GUA) and gluconic acid (GA). These carboxylic acids are very important building blocks for pharmaceutical, food, perfume or fuel industries [33]. Moreover, CO_2 and traces levels of hydrocarbon species (methane, ethane, acetaldehyde) were detected. Fig. 6 compares the selectivity results obtained for the studied photocatalysts Cr–TiO_2/ZeUI, Cr–TiO_2/SiO_2UI, TiO_2/ZeUI and TiO_2/SiO_2UI at the solvent composition of 10% H_2O/90% ACN. As can be seen from Fig. 6, the incorporation of chromium definitively helps to obtain more selective systems for carboxylic acids production. The addition of CH_3CN (ACN) has been reported to improve selectivity due to the "shield effect" driven by acetonitrile solvent [34]. In the photocatalytic process of epoxidation of light alkenes, acetonitrile (a weak base)

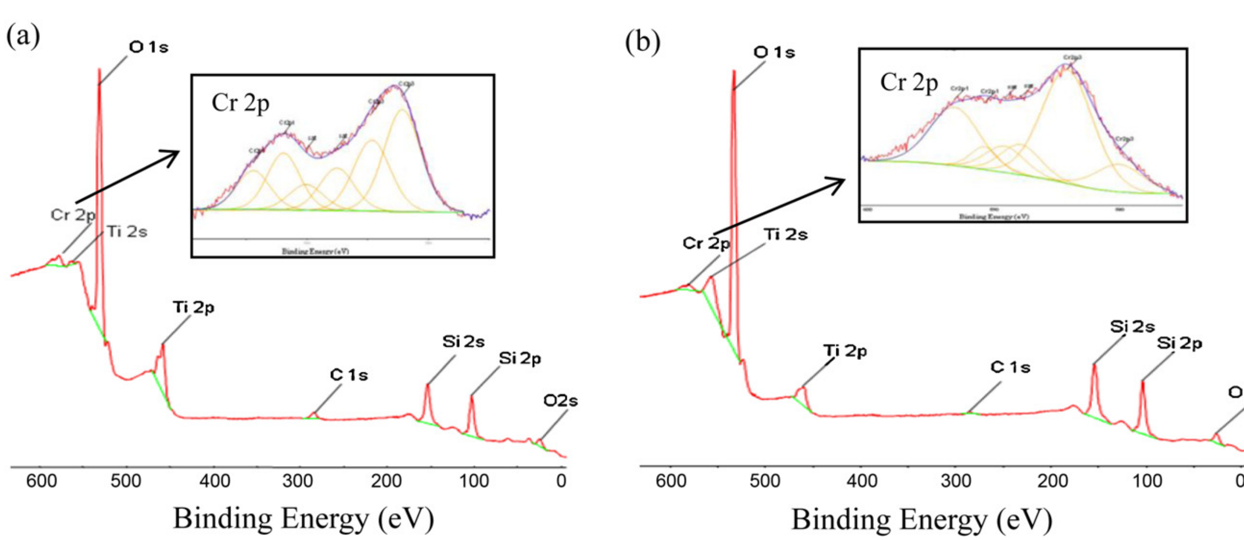

Fig. 5. XPS survey of Cr–TiO_2/ZeUI (a) and Cr–TiO_2/SiO_2UI (b) materials.

Table 4
Cr/Ti atomic ratios estimated from different techniques.

Photocatalyst	Cr/Ti atomic ratio			
	Nominal bulk content	Bulk content by XRF	Bulk content by ICP-MS	Surface content by XPS
$Cr–TiO_2/ZeUI$	0.09	0.11	0.10	0.26
$Cr–TiO_2/SiO_2UI$	0.09	0.09	0.08	0.43

stabilizes the reaction products by solvation inhibiting the proton transfer and at the same time preventing the formation of radical species that afford undesirable oxidation [35]. As it is seen, (Fig. 6), zeolite supported Cr doped titania is more selective to carboxylic acids than silica supported Cr doped titania in each interval time. Interestingly, in the first 5 min of illumination, no selectivity in the liquid phase is observed for these photocatalysts. In contrast, after 5 min of illumination the best selectivity results are obtained for titania supported systems (ca. 85% of selectivity for GUA + GA in the case of zeolite loaded titania and ca. 65% of selectivity in the case of titania loaded on silica). Appreciable selectivity for the chromium doped zeolite supported photocatalyst is obtained in 10 min of illumination (total selectivity for GUA + GA is 99.7% with the 8% of glucose conversion), whereas for Cr doped silica supported photocatalyst in the same illumination time total selectivity for GUA + GA is 84.9% with 9% of glucose conversion. Hence, the attribute of better selectivity properties is ascribed to zeolite supported photocatalyst during the whole reaction time (240 min). It could be correlated with the textural and structural characteristics of zeolite materials, the spherical shape of TiO_2, well-crystallized particles and the mixed oxidation states of chromium present in this photocatalyst (Cr^{3+}:Cr^{6+} = 59:41 surface atomic ratio). The influence of the chromium species on the selectivity could be also confirmed by better selectivity results obtained with $Cr–TiO_2/ZeUI$ than with $TiO_2/ZeUI$.

One important thing to highlight is the fact that any chromium leaching after the photocatalytic tests was not observed. XRF measurements after 240 min of photocatalytic reaction showed 0.11 and 0.09 Cr/Ti atomic ratio for $Cr–TiO_2/ZeUI$ and $Cr–TiO_2/SiO_2UI$ (which are comparable to the values from Table 4), respectively and the absence of Cr and Ti in the liquid phase after reaction.

There is no significant difference in the glucose conversion between studied chromium doped photocatalysts in the first 15 min of reaction. However, after illumination time reached 20 min much better degradation properties of $Cr–TiO_2/SiO_2UI$ are observed in comparison to $Cr–TiO_2/ZeUI$. After 240 min of reaction the conversion of glucose achieved by $Cr–TiO_2/SiO_2UI$ (79%) is almost two times higher in comparison with $Cr–TiO_2/ZeUI$ (44%). Therefore, a better degradation properties can be ascribed to titania supported on silica material. This strong oxidation properties could be also correlated with the predominant (82%) Cr^{6+} state in the $Cr–TiO_2/SiO_2UI$ sample. Better degradation properties can be also ascribed to TiO_2/SiO_2UI photocatalyst, which obtained better degradation rate in the first 20 min of illumination than $TiO_2/ZeUI$.

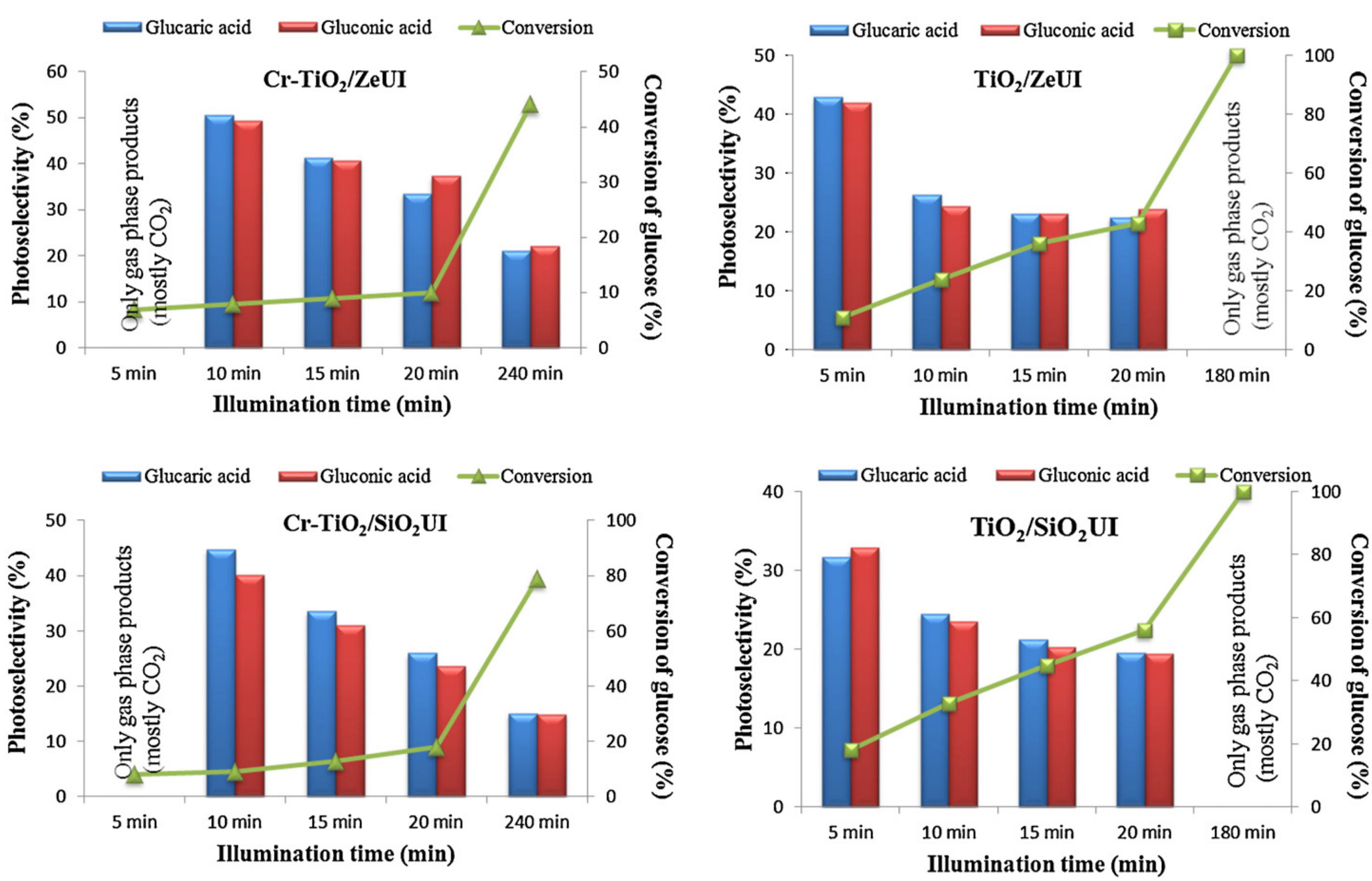

Fig. 6. Selectivity and conversion results for the photo-oxidation of glucose (reaction conditions: 150 mL of mother solution, $C_{glucose}$ = 2.8 mmol/L, 150 mg of photocatalyst, 30 °C, 1 atm., 125 W UV-lamp, H_2O:ACN = 10:90 v/v).

Table 5
Effect of solvent composition on glucose conversion and total selectivity for carboxylic acids (glucaric acid, gluconic acid) in the liquid phase (reaction conditions: 150 mL of mother solution, $C_{glucose}$ = 2.8 mmol/L, 150 mg of photocatalyst, 30 °C, 1 atm., 125 W UV-lamp).

Photocatalyst	Solvent composition					
	10% H_2O/90% ACN		50% H_2O/50% ACN		100% H_2O	
	Conversion [%]	ΣSelectivity [%]	Conversion [%]	ΣSelectivity [%]	Conversion [%]	ΣSelectivity [%]
Cr–TiO_2/ZeUI/20 min illumination	10	71	7	87	5	0
Cr–TiO_2/ZeUI/90 min illumination	24	46	8	77	6	0

Interestingly, after 240 min of reaction, the conversion of glucose achieved by Cr-free systems was 100% and no liquid phase products have been detected.

Therefore, solvent (water/ACN) optimization studies have been performed for Cr doped titania loaded zeolite. Table 5 compares selectivity and conversion results for different solvent mixtures: 10% H_2O/90% ACN, 50% H_2O/50% ACN and 100% H_2O after two interval reaction times, 20 min and 90 min of illumination. It is clearly seen that when the amount of water in the solvent mixture increases, the glucose conversion rate decreases. It has been also observed by Lopez-Tenllado et al. [36] in the photo-oxidation studies of crotyl alcohol to crotonaldehyde. The authors claim that the competition of water and crotyl alcohol for the adsorption sites of catalyst could be the reason of this decrease. In the case of selectivity to carboxylic acids, there has been no selectivity observed for 100% H_2O during the whole reaction. The best selectivity results has been obtained for 50% H_2O/50% ACN (87.3% and 77.1% after 20 and 90 min of illumination, respectively). Such water/ACN volume ratio has also been indicated as the mixture giving the highest selectivity for bulk TiO_2 reported previously [37]. It has been also observed that in the mixtures containing more than 10% of water the Cr–TiO_2 supported on zeolite photocatalyst is slightly more selective to gluconic acid (results not shown).

Photocatalytic properties of zeolite supported materials depends on the surface charge of zeolite as if the adsorption of substrates/products on the photocatalyst is an important factor that affects the photocatalytic activity/selectivity. Y type zeolites are negatively charged materials therefore they adsorb on the surface, by electrostatic attraction, cationic substrates and repulse anionic substrates [38]. This behavior can facilitate the selective photocatalytic oxidation of glucose, because the carboxylic acids under the reaction conditions (pH measurements show that oxidation of glucose leads to the formation of acidic compounds, since after 4 h of photocatalytic reaction the pH lowered from 6–7, depending on glucose solvent composition, to about 4–5) are repulsed preventing at the same time their complete photo-oxidation. Repulsion of the carboxylic acids from the photocatalyst surface is also observed for Cr doped silica photocatalyst (the same reaction products), but higher selectivity to carboxylic acids in the case of Cr–TiO_2/ZeUI photocatalyst indicates the more acidic character of the support that helps in the selective photo-oxidation process [39]. Moreover, the presence of acetonitrile in the solvent mixture helps to stabilize the carboxylic acids by solvation and suppress their further oxidation.

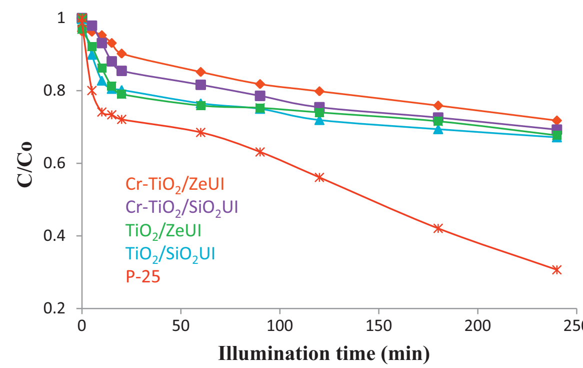

Fig. 7. Photocatalytic activity for phenol decomposition as a function of time (reaction condition: 150 mL of aqueous solution, 150 mg of photocatalyst, C_{phenol} = 50 ppm, 125 W UV-lamp).

Phenol-derived compounds	Retention time (min)
Hydroquinone	1.9
1,4-Benzoquinone	2.2
Resorcinol	2.4
Catechol	3.2
1,2,4-Benzenetriol	3.8

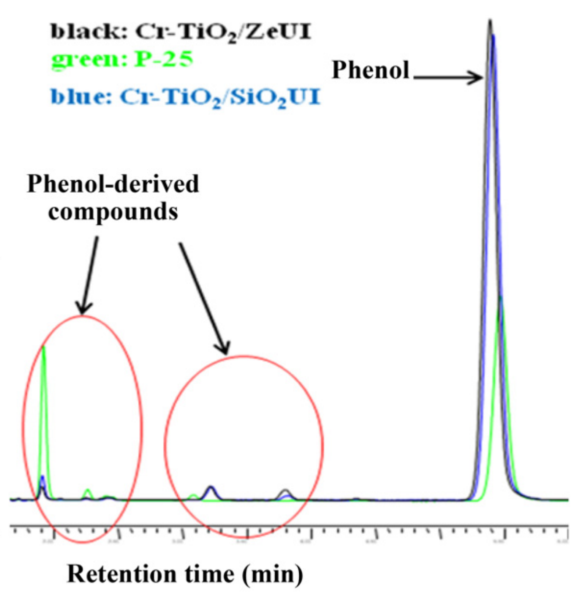

Fig. 8. HPLC–MS representative analysis for 240 min of photocatalytic degradation of phenol.

3.2.2. Aqueous phase photodegradation of phenol

Photocatalytic activity of synthesized catalytic samples have been also investigated in phenol degradation. To verify the photocatalytic abilities of the samples synthesized by our methodology the experiments were conducted during 4 h of illumination. No appreciable phenol degradation was found in the absence of UV irradiation or catalyst. There is no appreciable difference in phenol degradation rate (Fig. 7) achieved for the synthesized photocatalysts, that after 240 min of illumination have reached ca. 30%.

Comparing with the phenol degradation results under the same reaction conditions obtained for the systems without Cr (ca. 33% of degradation) it can be deduced that Cr doping has no significant effect on the photocatalytic degradation rate in this reaction. The most active photocatalyst was the commercially available Evonik P-25, which achieved almost 70% of phenol degradation. Unfortunately, P-25 is leaving (Fig. 8) in the aqueous phase high quantities of phenol-derived harmful compounds (hydroquinone, 1,4-benzoquinone, resorcinol, catechol and 1,2,4-benzenetriol), apart from phenol, while in the case of synthesized photocatalysts the amount of these compounds is negligible especially for Cr–TiO_2/SiO_2UI photocatalyst which is converting phenol with very high selectivity into carbon dioxide and water.

4. Conclusions

Cr modified titania photocatalysts were synthesized following the improved wet impregnation method assisted by ultrasonic irradiation. The application of ultrasonic irradiation also during the rotary evaporation step resulted in spherically shaped nanomaterials with a good elemental distribution. A shift in the band gap energy to the visible region was produced in the chromium doped photocatalysts in comparison to the TiO_2 neat catalyst. Modification of the initial chromium oxidation state Cr (III) to Cr (VI) occurring during the annealing of the solids was evidenced by XPS spectroscopy. Materials were found to be photocatalytically active (without metal leaching) in the selective partial oxidation of glucose to carboxylic acids (GA + GUA). The most selective system was zeolite supported photocatalyst (Cr–TiO_2/ZeUI) that after 20 min of illuminations achieved 87.3% of selectivity for a solvent composition of 50% H_2O/50% ACN. It has been found that reaction conditions, particularly solvent composition and short illumination times (10 min.), have also considerable effect on the activity/selectivity of tested photocatalysts.

Cr doping has no important effect on the mineralization rate of phenol. It has also been suggested that supporting Cr–TiO_2 on silica remarkably reduces formation (increases the mineralization to carbon dioxide and water) of phenol by-products in aqueous phase.

Acknowledgements

This research was supported by a Marie Curie International Reintegration Grant within the 7th European Community Framework Programme. This scientific work was financed from the 2012 to 2014 science financial resources, granted for the international co-financed project implementation (Project No. 473/7.PR/2012, Ministry of Science and Higher Education of Poland).

References

[1] B. Sun, E.P. Reddy, P.G. Smirniotis, Applied Catalysis B 57 (2005) 139–149.
[2] M. Illie, B. Cojocaru, V.I. Parvulescu, H. Garcia, International Journal of Hydrogen Energy 36 (2011) 15509–15518.
[3] J. Zhu, Z. Deng, F. Chen, J. Zhang, H. Chen, M. Anpo, J. Huang, L. Zhang, Applied Catalysis B 62 (2006) 329–335.
[4] X. Fan, X. Chen, S. Zhu, Z. Li, T. Yu, J. Ye, Z. Zou, Journal of Molecular Catalysis 284 (2008) 155–160.
[5] A. Di Paola, E. Garcia-Lopez, S. Ikeda, G. Marci, B. Ohtani, L. Palmisano, Catalysis Today 75 (2002) 87–93.
[6] J.C. Yu, G. Li, X. Wang, X. Hu, C.W. Leung, Z. Zhang, Chemical Communications 25 (2006) 2717–2719.
[7] J.B. Yin, X.P. Zhao, Journal of Physical Chemistry B 110 (2006) 12916–12925.
[8] Ch.C. Wang, C.K. Lee, M.D. Lyu, L.Ch. Juang, Dyes and Pigments 76 (2007) 817–824.
[9] A.Y. Shan, T.I.M. Gazi, S.A. Rashid, Applied Catalysis A 389 (2010) 1–8.
[10] J.C. Colmenares, in: M. Song (Ed.), Catalysis: Principles, Types and Applications, Nova Science Publishers Inc., New York, 2011, pp. 101–165.
[11] M.V. Shankar, S. Anandan, N. Venkatachalam, B. Arabindoo, V. Murugesan, Chemosphere 63 (2006) 1014–1021.
[12] S. Sankararaman, K.B. Yoon, T. Yabe, J.K. Kochi, Journal of the American Chemical Society 113 (1991) 1419–1420.
[13] H. Kobayashi, T. Komanoya, S.K. Guha, K. Hara, A. Fukuoka, Applied Catalysis A 409/410 (2011) 13–20.
[14] C.S. Goh, K.T. Lee, S. Bhatia, Bioresource Technology 107 (2010) 7362–7367.
[15] S.G. Li, S.P. Xu, S.Q. Liu, C. Yang, Q.H. Lu, Fuel Processing Technology 85 (2004) 1201–1211.
[16] H.X. Hao, L.J. Guo, X. Mao, X.M. Zhang, X.J. Cheng, International Journal of Hydrogen Energy 28 (2003) 55–64.
[17] X. Fu, X. Wang, D.Y.C. Leung, W. Xue, Z. Ding, H. Huang, X. Fu, Catalysis Communications 12 (2010) 184–187.
[18] J.H. Bang, K.S. Suslick, Advanced Materials 22 (2010) 1039–1059.
[19] S.Y. Kim, T.S. Chang, ChH. Shin, Catalysis Letters 118 (2007) 224–230.
[20] M. Zhou, J. Yu, B. Cheng, Journal of Hazardous Materials 137 (2006) 1838–1847.
[21] L. Zhou, W. Wang, L. Zhang, Journal of Molecular Catalysis A 268 (2007) 195–200.
[22] F. Tomful, Applied Surface Science 258 (2011) 1836–1848.
[23] Q. Wu, J. Ouyang, K. Xie, L. Sun, M. Wang, Ch. Lin, Journal of Hazardous Materials 199/200 (2012) 410–417.
[24] S. Sakthivel, H. Kisch, Angewandte Chemie International Edition 42 (2003) 4908–4911.
[25] Ch. Wang, H. Shi, Y. Li, Applied Surface Science 258 (2012) 4328–4333.
[26] R. Lopez, R. Gomez, S. Oros-Ruiz, Catalysis Today 166 (2011) 159–165.
[27] H. Kato, A. Kudo, Journal of Physical Chemistry B 106 (2002) 5029–5034.
[28] W. Choi, A. Termin, M.R. Hoffman, Journal of Physical Chemistry 98 (1994) 13669–13679.
[29] N. Serpone, Journal of Physical Chemistry B 110 (2006) 24287–24293.
[30] J.C. Colmenares, A. Magdziarz, M.A. Aramendia, A. Marinas, J.M. Marinas, F.J. Urbano, J.A. Navio, Catalysis Communications 16 (2011) 1–6.
[31] D.I. Kondarides, A. Patsoura, X.E. Verykios, Journal of Advanced Oxidation Technology 13 (2010) 116–123.
[32] Y. Li, J. Wang, S. Peng, G. Lu, S. Li, International Journal of Hydrogen Energy 35 (2010) 7116–7126.
[33] J.C. Colmenares, R. Luque, J.M. Campelo, F. Colmenares, Z. Karpinski, A.A. Romero, Materials 2 (2009) 2228–2258.
[34] Y. Shiraishi, T. Hirai, Journal of Photochemistry and Photobiology 9 (2008) 157–170.
[35] A. Maldotti, A. Molinari, Topics in Current Chemistry 303 (2011) 185–216.
[36] F.J. Lopez-Tenllado, A. Marinas, F.J. Urbano, J.C. Colmenares, M.C. Hidalgo, J.M. Marinas, J.M. Moreno, Applied Catalysis B: Environmental 128 (2012) 150–158.
[37] J.C. Colmenares, A. Magdziarz, A. Bielejewska, Bioresource Technology 102 (2011) 11254–11257.
[38] G. Zhang, W. Choi, S.H. Kim, S.B. Hong, Journal of Hazardous Materials 188 (2011) 198–205.
[39] D. An, A. Ye, W. Deng, Q. Zhang, Y. Wang, European Journal of Chemistry 18 (2012) 2938–2947.